atoms

MDPI

Article

The Binary-Encounter-Bethe Model for Computation of Singly Differential Cross Sections Due to Electron-Impact Ionization

Pankaj Garkoti [1], Meetu Luthra [1], Kanupriya Goswami [2], Anand Bharadvaja [1,*] and Kasturi Lal Baluja [3,†]

[1] Department of Physics, Bhaskaracharya College of Applied Sciences, University of Delhi, New Delhi 110075, India; garkotipankaj@gmail.com (P.G.); meetu.luthra@bcas.du.ac.in (M.L.)
[2] Department of Physics, Keshav Mahavidyalaya, University of Delhi, New Delhi 110034, India; kanupriyagoswami@keshav.du.ac.in
[3] Department of Physics and Astrophysics, University of Delhi, Delhi 110007, India; kl_baluja@yahoo.com
* Correspondence: anand_bharadvaja@yahoo.com
† Retired Professor.

Abstract: In the present work, we assess the effectiveness of singly differential cross sections (SDCS) due to electron-impact ionization by invoking the binary-encounter-Bethe (BEB) model on various atomic and molecular targets. The computed results were compared with the experimental and theoretical data. A good agreement was observed between the present and the available results. This agreement improves as the incident energy of the projectile increases. The model can be applied to compute the SDCS for the ions produced due to the electron-impact dissociative ionization process and the average energy due to the secondary electrons. Both these quantities are of interest in plasma processing and radiation physics.

Keywords: electron-impact ionization; cross sections; singly differentiated cross sections; energy deposition; semiempirical methods; differential oscillator strengths; BEB model

Citation: Garkoti, P.; Luthra, M.; Goswami, K.; Bharadvaja, A.; Baluja, K.L. The Binary-Encounter-Bethe Model for Computation of Singly Differential Cross Sections Due to Electron-Impact Ionization. *Atoms* **2022**, *10*, 60. https://doi.org/10.3390/atoms10020060

Academic Editors: Dhanoj Gupta, Suvam Singh, Paresh Modak and Eugene T. Kennedy

Received: 14 April 2022
Accepted: 27 May 2022
Published: 6 June 2022

1. Introduction

The electron-impact ionization is one of the most elementary processes in basic and applied physics [1,2]. The ionization cross sections due to electron-impact are used as input parameters in the study of various physical phenomena such as radiation damage, [3] planetary atmospheres [4,5], and plasma processing [6,7]. Ionization SDCS are also the input parameters for the Monte-Carlo based simulations to model the track of energetic secondary particles in biological matter [8]. The secondary electrons produced during ionization can inflict significant damage to biomolecules [9,10]. Hence, reliable models are required to estimate the energy deposition due to electron-impact ionization. This requires computation of SDCS for a variety of targets over a wide energy range.

Various ab initio and semiempirical formulations that exist to compute electron-ionization cross sections have their own merits and limitations. The ab initio approaches such as the convergent close-coupling (CCC) approach [11,12] and the R-matrix with pseudostates [13] aim to compute the scattering cross sections directly from the quantum mechanical first principles. The applicability of these methods has so far been confined to simple diatomic targets because the computational complexity becomes prohibitive due to the target size and the basis set used [14]. Furthermore, these methods suffer from issues such as linear dependency [13] and ill conditioning [14].

The semiempirical approaches [15], on the other hand, are relatively easy to apply and perform quite well even for complicated targets. The models such as the binary-encounter-dipole (BED) and binary-encounter-Bethe (BEB) of Kim and Rudd [16], the Jain-Khare (JK) model and its modified form [17,18], the Deutsch-Märk model [19,20], and several modified forms of the BEB model [21,22] are examples of semiempirical formulations commonly employed to compute ionization cross sections. The BED and JK models require differential

oscillator strength (DOS) values of the target as an input parameter. This hinders the applicability of these methods, as calculating DOS even for simple targets is a tedious process [23]. The BEB model is a simplification of the BED model in which the DOS term is approximated by a simple function of W (secondary electron energy). The BED and BEB models are briefly discussed in the next section. A detailed review of the BED model and related techniques can be found in [24]. This paper is organized as follows: Section 2 discusses the BEB and BED models. The computational aspects, resultsm and observations are presented in Section 3. The discussion is presented in Section 4.

2. Methodology

2.1. The BED Model

The binary-encounter-dipole, or BED model of Kim and Rudd [16] combines the aspects of binary-encounter theory with the dipole interactions of the Bethe theory and the electron exchange effects proposed by L. Vriens [25]. The overall accuracy of this model is accepted to be within 10% or closer to the experimental values. The SDCS in the BED model is given by [16]:

$$\frac{d\sigma(W,T)}{dW} = \frac{S_i}{B_i(t_i+u_i+1)}\left\{\frac{(N_i/N)-2}{t_i+1}\left(\frac{1}{w_i+1}+\frac{1}{t_i-w_i}\right)\right. \\ \left. +(2-N_i/N)\left[\frac{1}{(w_i+1)^2}+\frac{1}{(t_i-w_i))^2}\right]+\frac{\ln t_i}{N(w_i+1)}\frac{df(w_i)}{dw_i}\right\} \quad (1)$$

Here, $\frac{d\sigma(W,T)}{dW}$ denotes the SDCS, and T refers to the energy of the projectile electron. The $w_i = W_i/B_i$, $t_i = T/B_i$, $u_i = U_i/B_i$, $S_i = 4\pi a_0^2\, N_i\, (R/B_i)^2$, and $\frac{df(w)}{dw}$ is the differential oscillator strength. The N_i is the occupation number of the i-th orbital. B_i, W_i, and U_i are the binding energy, ejected electron energy, and the average kinetic energy of the electron in the i-th orbital, respectively. The total SDCS is obtained by summing over all those orbitals that satisfy the condition $T \geq B_i$.

2.2. The BEB Model

The SDCS in the BEB model are obtained by simplifying Equation (1), where $\frac{df(w_i)}{dw_i}$ is replaced by $\frac{N_i}{(w_i+1)^2}$ [16]. Thus, the SDCS is given by:

$$\frac{d\sigma(W,T)}{dW} = \frac{S_i}{B_i(t_i+u_i+1)}\left\{\frac{(N_i/N)-2}{t_i+1}\left(\frac{1}{w_i+1}+\frac{1}{t_i-w_i}\right)\right. \\ \left. +(2-N_i/N)\left[\frac{1}{(w_i+1)^2}+\frac{1}{(t_i-w_i))^2}\right]+\frac{N_i\ln t_i}{N(w_i+1)^3}\right\} \quad (2)$$

This leads to a very simple and convenient analytical form of total ionization cross sections (TICS):

$$\sigma_i(t_i) = \frac{S_i}{t_i+u_i+1}\left\{\frac{Q_i}{2}\left(1-\frac{1}{t_i^2}\right)\ln t_i\right. \\ \left. +(2-Q_i)\left[\left(1-\frac{1}{t_i}\right)-\frac{\ln t_i}{t_i+1}\right]\right\} \quad (3)$$

Here, $Q_i = N_i/N$. In the BEB approximation, Q_i is taken to be unity. Despite being simple, Equation (3) shows excellent agreement with the experimental data [26]. The advantage of invoking the BEB model is that the expressions for SDCS or TICS are given by a very simple analytical expression and require input parameters such as B, U, and N for different occupied orbitals. These parameters obtained at Hartree-Fock level have yielded excellent results for a large number of targets even with the modest basis set. The BEB model is found to give reliable results for the TICS but its effectiveness has

not yet been investigated established for SDCS. The SDCS for some targets have been presented previously but not in a manner that highlights and compares the accuracy of BEB. For example, the SDCS for H-atom at 60 eV has been presented in [16]. The SDCS are useful in the calculation of the average energy of the secondary electrons W_{av}. Hence, it is important to evaluate the performance of the SDCS given by the BEB model.

2.3. Average Secondary Electron Energy

The average energy of secondary electrons, W_{av}, is an extremely important quantity in fields such as biophysics and plasma processing and is associated with the SDCS. The secondary electrons produced due to electron-impact ionization are responsible for the damage in tissues and genetic material [27]. The W_{av} can be obtained using the SDCS:

$$W_{av} = \int_0^{(T-B)/2} W \frac{d\sigma}{dW} \, dW \Big/ \int_0^{(T-B)/2} \frac{d\sigma}{dW} \, dW \tag{4}$$

In this work, we have used the BEB model to compute the SDCS and, hence, the W_{av}.

3. Computational Details and Results

The targets considered in this work were optimized using the Gaussian software [28] at Hartree-Fock (HF) level using 6-311G* basis set. This generated the parameters (B_i, U_i, and N_i) required to compute the SDCS. We present the SDCS for simple targets (H, He, H_2, N_2, H_2O, and C_2H_2) and a few complex targets (C_2H_5OH, pyrimidine, tetrahydrofuran, etc.). Wherever possible, comparisons with available experimental and theoretical data have been made to illustrate the extent to which the BEB model is accurate and reliable.

3.1. Hydrogen Atom (H)

The electron-impact ionization of the H atom is relevant in the modeling of plasmas [29], stellar atmospheres [30], and planetary atmospheres [31]. The simplicity of the H atom makes it an ideal system to test any theory attempting to predict ionization cross sections. The BEB-SDCS for the H-atom at various energies are shown in Figure 1a–f. The results were compared with the experimental values of Shyn [32] and the CCC approach-based results of Mori et al. [33]. The experimental results of Shyn had an uncertainty of ±20%. The CCC results of Mori et al. [33] were obtained after including 173 states in the close-coupling expansion. These are the most accurate theoretical results for the H-atom to date. We see a good agreement between the BEB and CCC results at different incident energies and secondary electron energies (W). However, both the theoretical results were lower than experimental results but still lay close to the experimental uncertainties at different energies.

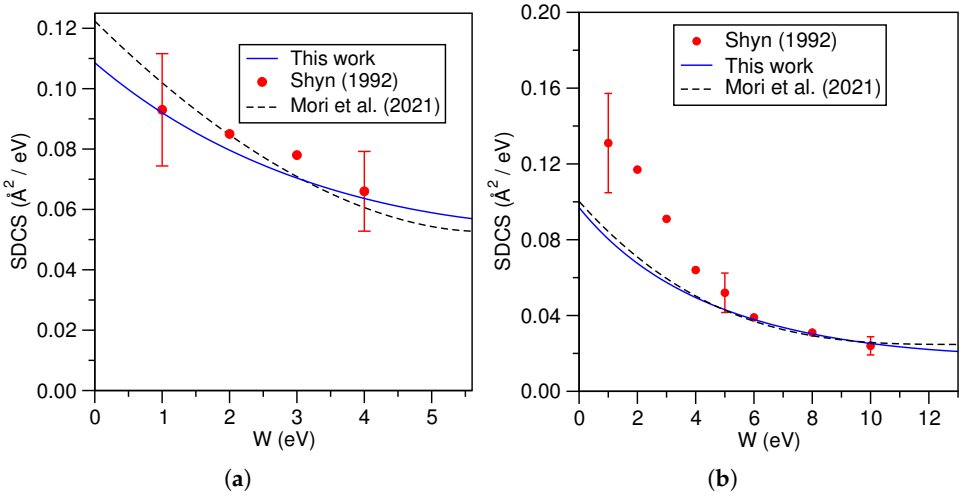

Figure 1. *Cont.*

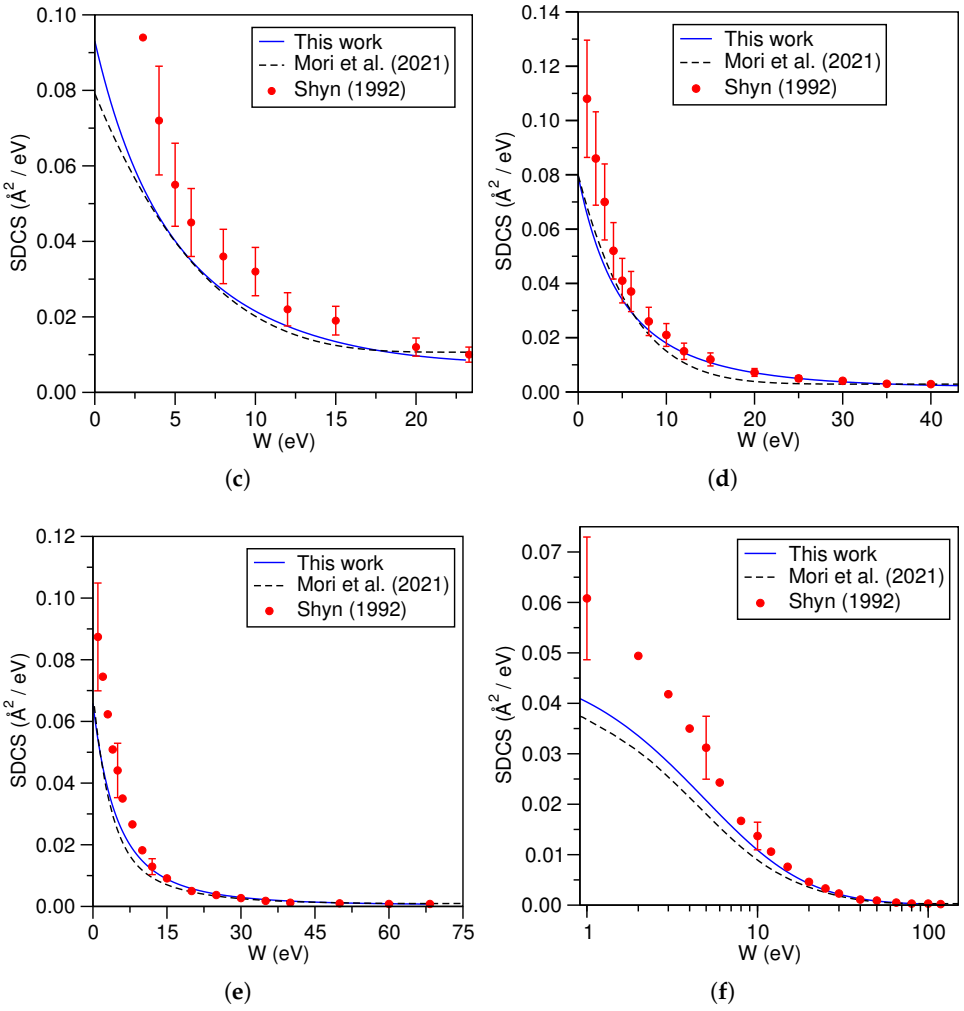

Figure 1. Electron-impact SDCS for H-atom at different primary electron energies (**a**) T = 25 eV, (**b**) T = 40 eV, (**c**) T = 60 eV, (**d**) T = 100 eV, (**e**) T = 150 eV, and (**f**) T = 250 eV. The present results are represented by solid lines, the dashed lines represent the results of Mori et al. [33], and the filled circles represent the experimental measurements of Shyn [34].

3.2. Helium Atom (He)

The BEB-SDCS for the He-atom at various energies are shown in Figure 2a–d. The BEB model results are compared with theoretical results of Mori et al. [33] at 40 eV and 100 eV. We again notice a satisfactory agreement between the present and CCC results [33]. This is encouraging, as the CCC approach is quite complex, sophisticated, and requires large computational resources. A concordance was observed with the experimental data of Opal et al. [35] at 100 eV, 200 eV, and 500 eV and Röder et al. [36] at 40 eV.

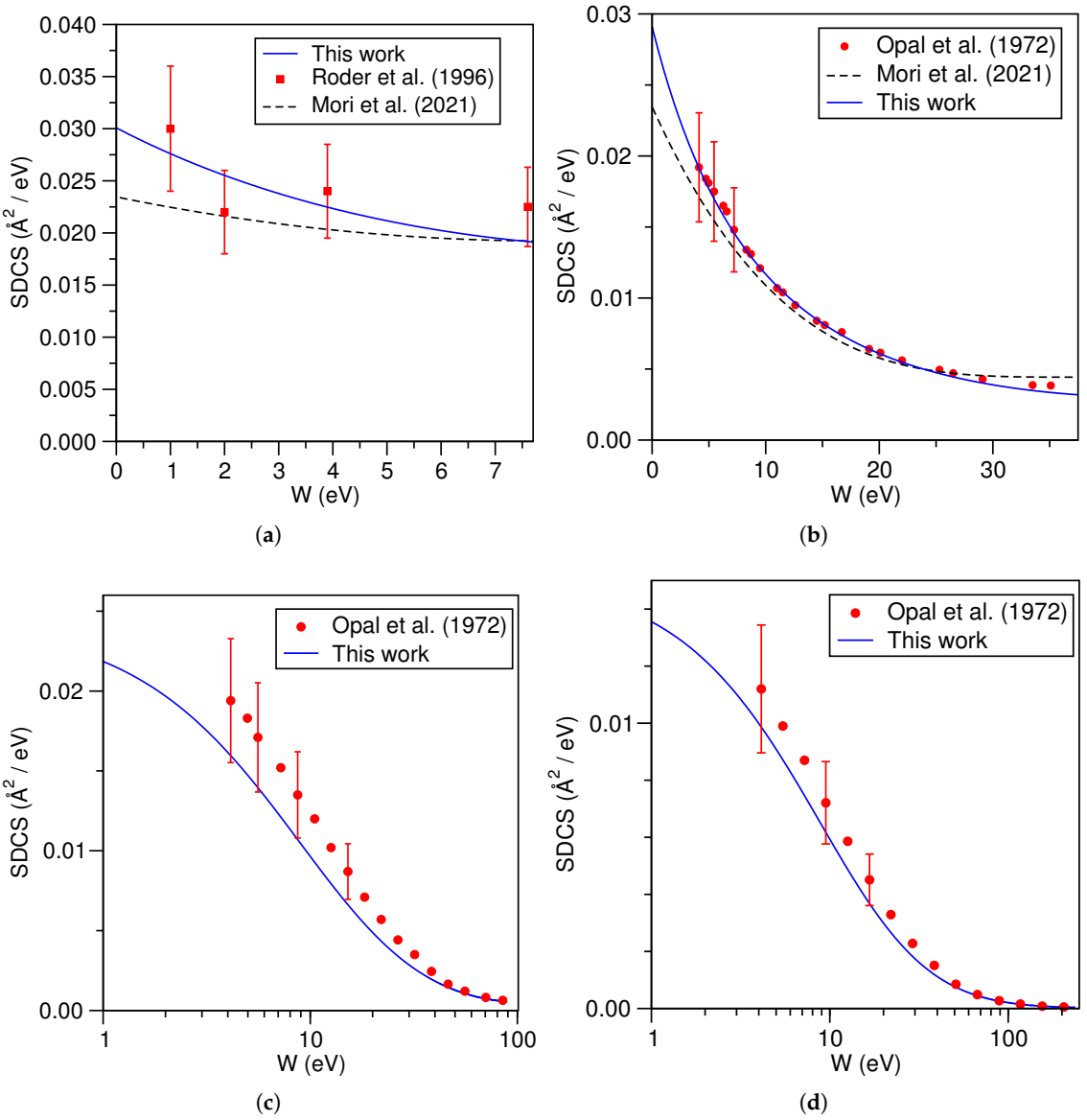

Figure 2. Electron-impact SDCS for electron-impact ionization of He-atom at a primary electron energy of (**a**) T = 40 eV, (**b**) T = 100 eV, (**c**) T = 200 eV, and (**d**) T = 500 eV. The solid lines represent the present results, the dashed lines represent the theoretical results of Mori et al. [33], the filled circles represent the experimental measurements of Opal et al. [35], and the filled squares represent the experimental results of Röder et al. [36].

3.3. Molecular Hydrogen (H_2)

The electron impact ionization SDCS for H_2 given by the BEB model for various incident energies are shown in Figure 3a–d. The experimental measurements are from Shyn et al. [32], with a reported uncertainty of ±16%. We have also compared the present results with the CCC theory-based results of Mori et al. [33]. The SDCS given by the BEB model for H_2 showed satisfactory agreement with both the experimental measurements and the CCC results at different energies [33].

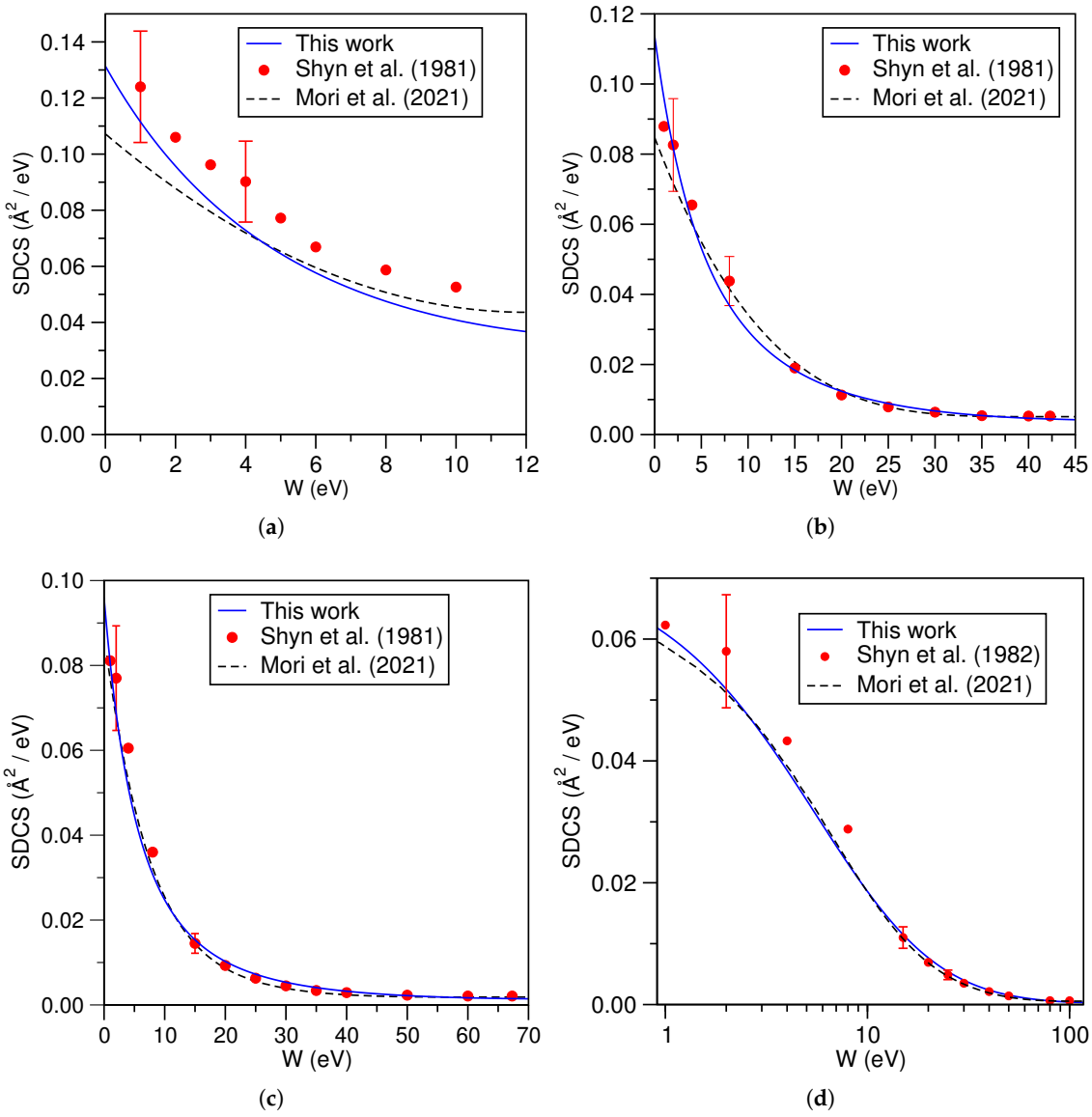

Figure 3. Electron-impact SDCS for H_2 at a primary electron energy of (**a**) T = 40 eV, (**b**) T = 100 eV, (**c**) T = 150 eV, and (**d**) T = 250 eV. The solid lines represent the present results, the dashed lines are the results of Mori et al. [33], and the filled circles are the experimental measurements of Shyn et al. [32].

3.4. Molecular Nitrogen (N_2)

Ionization cross sections for N_2 are relevant in modeling atmospheric plasmas and the interactions of high energy charged particles with the atmosphere (for example, the northern lights) [37,38]. The BEB-SDCS for various impact energies are shown in Figure 4a–d along with the experimental as well as the theoretical data. The experimental cross sections are from Opal et al. [35] and the theoretical results are from Pal et al. [39]. Pal and coworkers used a Jain-Khare semiempirical approach for the calculation of SDCS in their work. The SDCS given by the BEB model were in better agreement with the experimental values than Pal et al. [39].

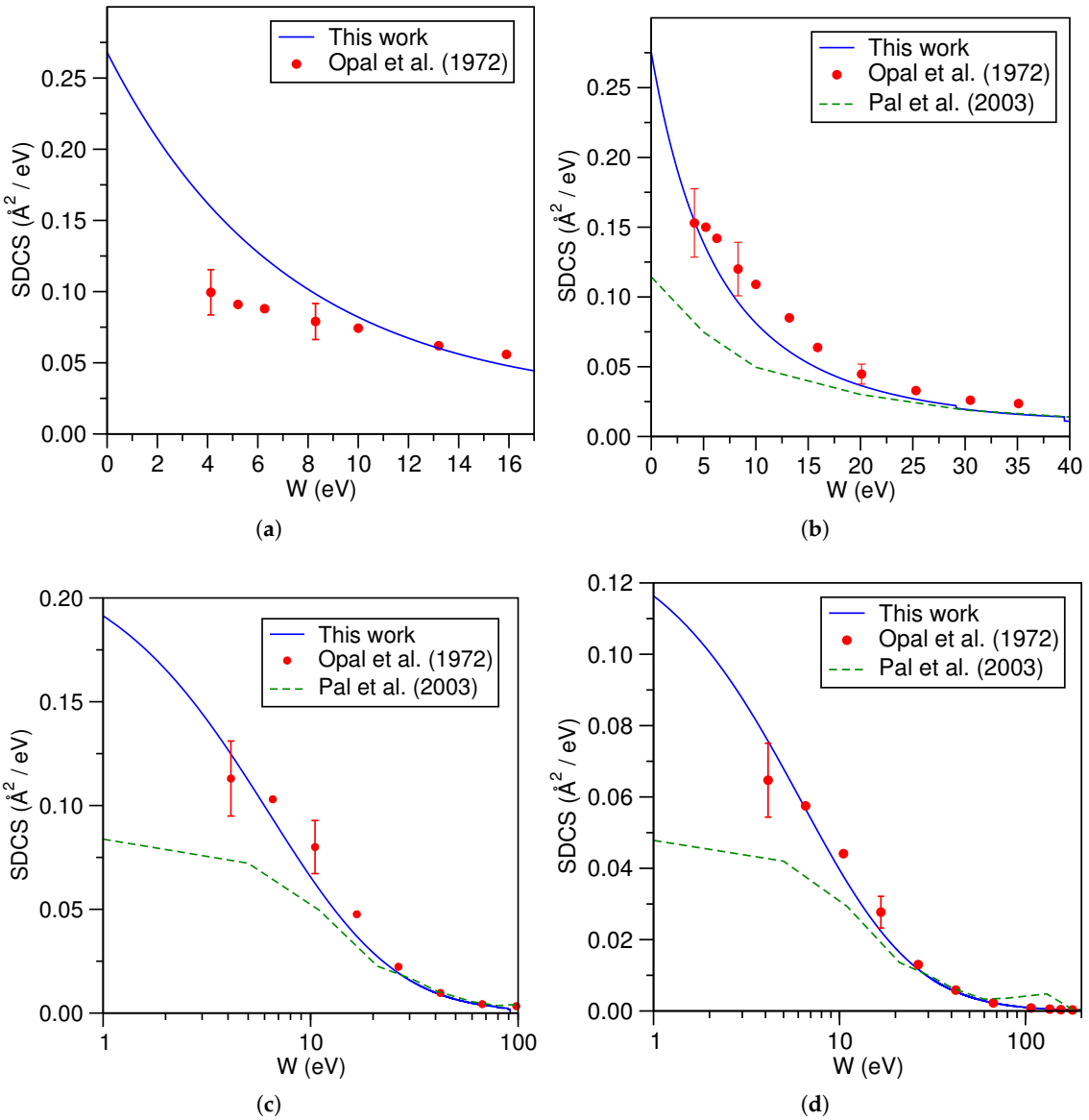

Figure 4. Electron-impact SDCS for N_2 at a primary electron energy of (**a**) T = 50 eV, (**b**) T = 100 eV, (**c**) T = 200 eV, and (**d**) T = 500 eV. The solid lines represent the present results, the dashed lines are the results of Pal et al. [39], and the filled circles are the experimental measurements of Opal et al. [35].

3.5. Molecular Oxygen (O_2)

Oxygen ionization cross sections are of significance in modeling atmospheric plasmas and the interaction of high energy charged particles with the atmosphere [40]. Electron impact ionization also plays a role in the inter-conversion between ozone and oxygen in the atmosphere [41]. The BEB-SDCS for an oxygen molecule at various incident energies of 50 eV, 100 eV, 200 eV, and 500 eV are shown in Figure 5a–d. The experimental cross sections are from Opal et al. [35], and the theoretical data is from Pal et al. [39] computed using a JK semiempirical approach. The SDCS given by the BEB model were in good agreement with the experimental values and better than those determined from the JK semiempirical approach [39].

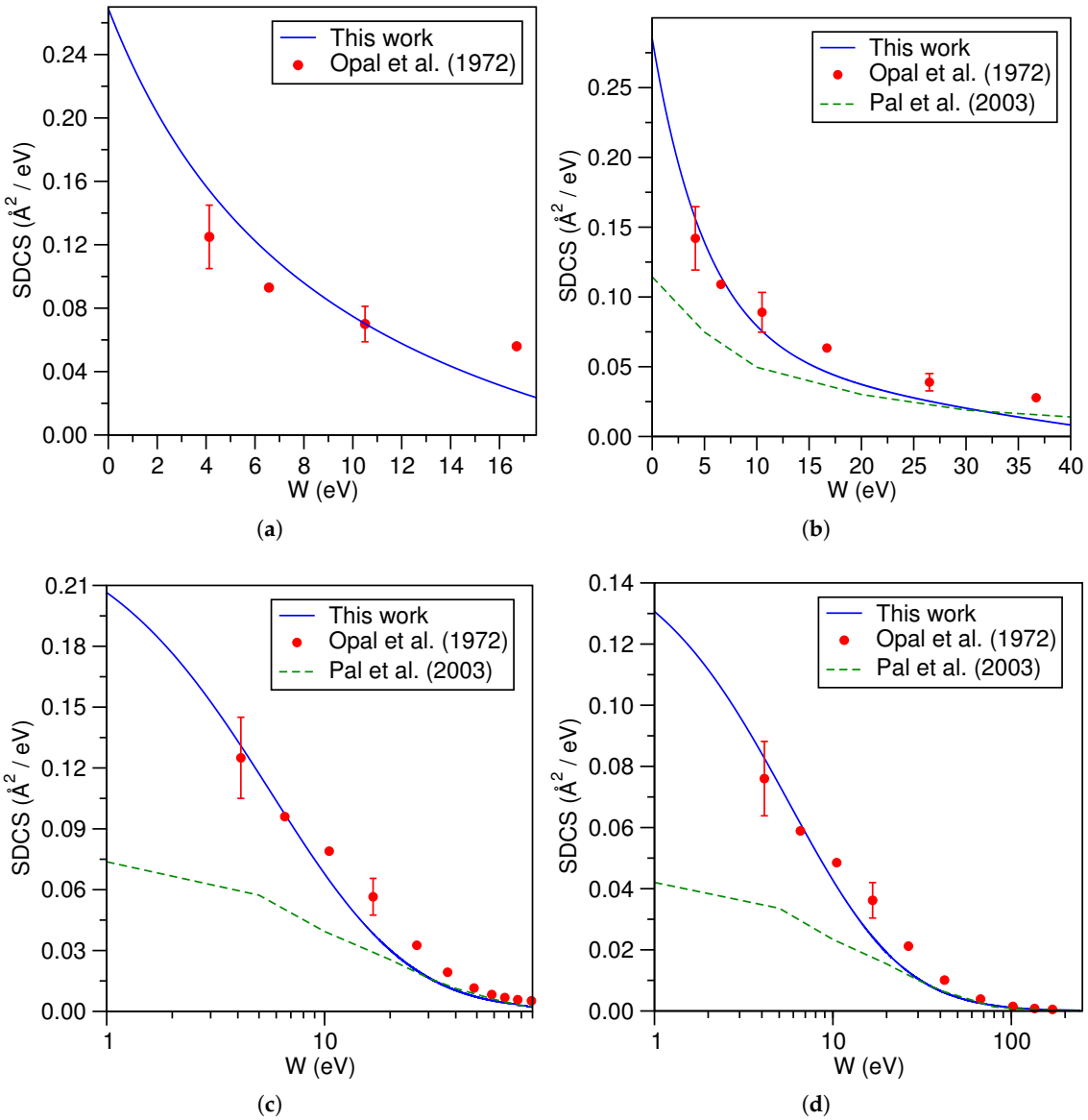

Figure 5. Electron-impact SDCS for O_2 at a primary electron energy of (**a**) T = 50 eV, (**b**) T = 100 eV, (**c**) T = 200 eV, and (**d**) T = 500 eV. The solid lines represent the present results, the dashed lines are the results of Pal et al. [39], and the filled circles are the experimental measurements of Opal et al. [35].

3.6. Water (H_2O)

The BEB-SDCS for H_2O at various incident energies are shown in Figure 6a–d. The electron-impact SDCS are of use in determination of the rotational abundance of water in cometary atmospheres and the modeling of combustion products from fossil fuels [42]. Since it is present in living tissues, the ionization cross sections for water can be used to obtain a rough estimate of the energy deposition and damage caused by the ionizing radiation in biological matter [43,44]. A good agreement is observed between experimental results of Bolorizadeh et al. [45], Opal et al. [35], and the present results. These results improved as the energy of the primary electron increased.

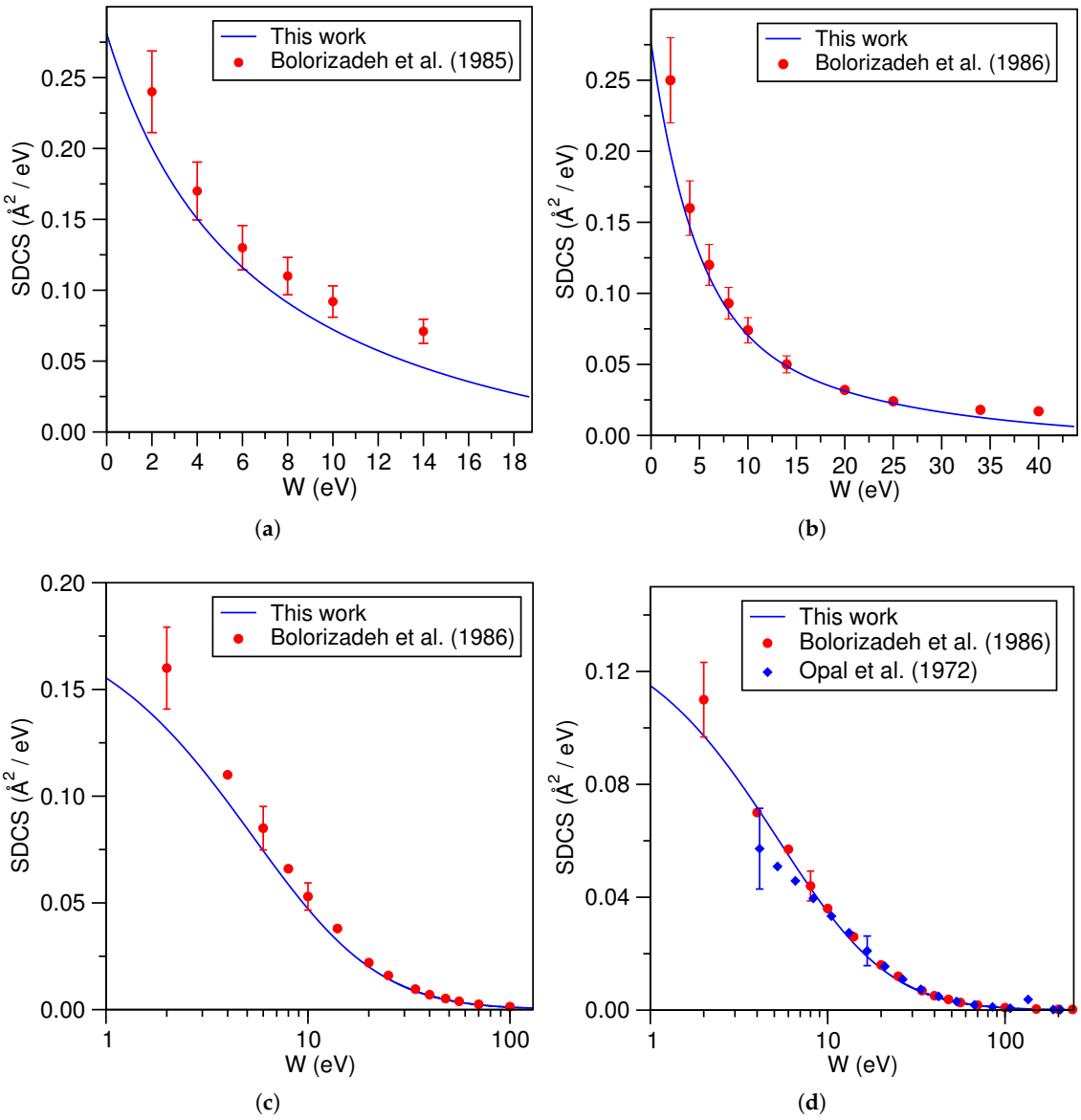

Figure 6. Electron-impact SDCS for H_2O at a primary electron energy of (**a**) T = 50 eV, (**b**) T = 100 eV, (**c**) T = 200 eV, and (**d**) T = 500 eV. The solid lines represent the present results, the filled circles are the experimental measurements of Bolorizadeh et al. [45], and the filled quadrilaterals are the experimental measurements of Opal et al. [35].

3.7. Acetylene (C_2H_2)

Acetylene plasmas find use in various fields such as the production of fullerenes [46] and in nanoscience for the production of carbon nanoparticles [47]. Several kinds of simple hydrocarbons, including acetylene are present in interstellar clouds [48]. The fact that simple hydrocarbons form as a result of astrophysical processes has important implications for astrobiology [49]. The availability of accurate electron-impact cross sections of these simple hydrocarbons aids the study of the chemical evolution of the matter present in interstellar meda. Electron-impact ionization data for acetylene are also important in simulations of fusion plasmas for reactors, which use graphite as the wall material [50]. The BEB-SDCS for C_2H_2 at incident energies are shown in Figure 7a,b. We have also included the recent theoretical work of Pal et al. [51].

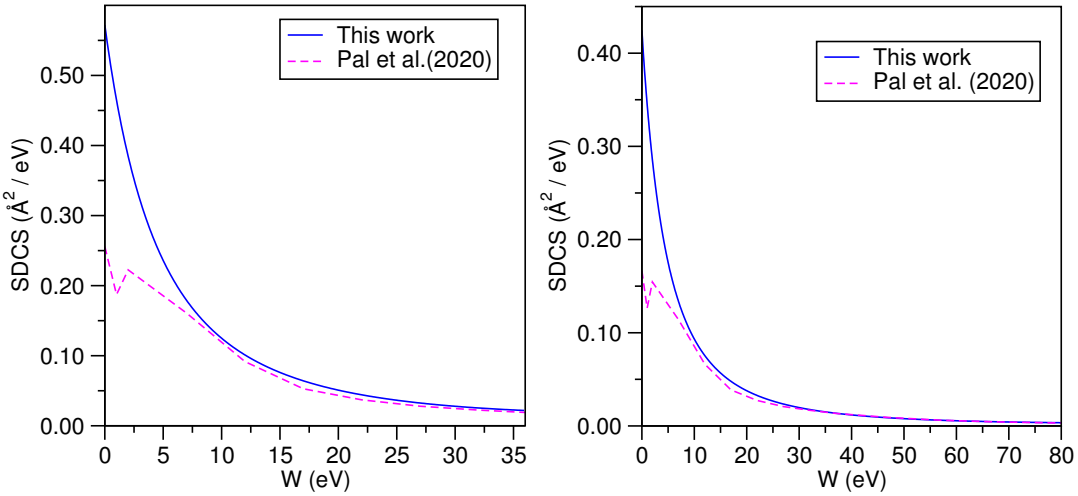

Figure 7. Electron-impact SDCS for C_2H_2 at (**a**) T = 100 eV and (**b**) T = 200 eV. The solid lines represent the present work, and the dashed lines represent the theoretical data of Pal et al. [51], computed using the JK semiempirical approach.

3.8. Ethanol (C_2H_5OH)

Ethanol is considered an alternative to traditional combustion fuels. Reliable ionization cross sections are required in plasma simulations of the combustion of ethanol in alternative fuel engines [52]. Ethanol is also found in interstellar environments and plays a significant part in the formation of organic compounds [53]. The BEB-SDCS for electron-impact ionization of ethanol are presented at various primary energies in Figure 8a,b. No experimental data were available to compare the present and other theoretical results [51]. Therefore to assess the quality of present results, we integrated the SDCS to obtain the TICS at specific energies. The integrated values of SDCS at 100 eV and 200 eV were in excellent agreement with the experimental results of Nixon et al. and Rejoub et al. [54,55]. The TICS of Pal et al. from the modified JK model [51] were higher than the experimental values at 100 eV and 200 eV. This provides us with the confidence to conclude that the present results can serve as a benchmark for future studies. The computed TICS are displayed in Figure 9.

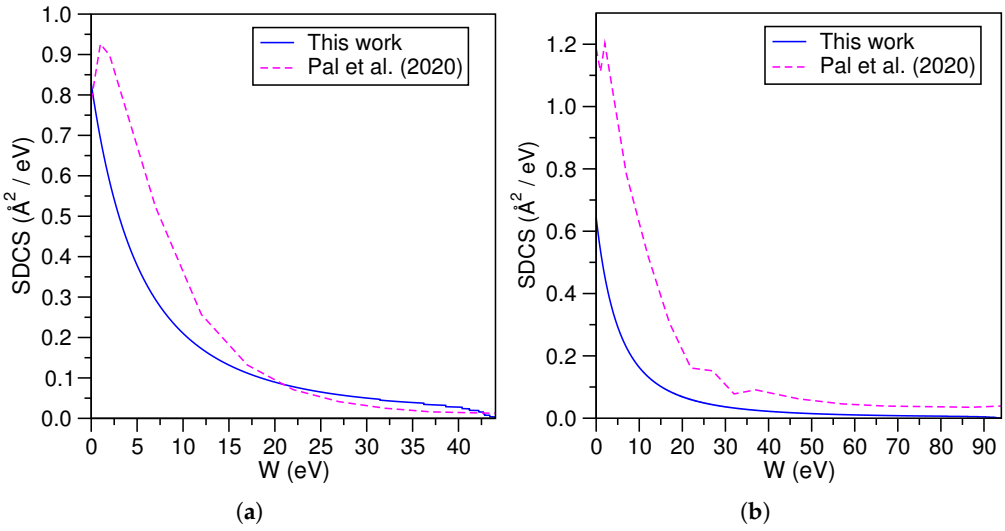

Figure 8. Electron-impact SDCS for C_2H_5OH at (**a**) T = 100 eV and (**b**) T = 200 eV. The solid lines represent the present work, and the dashed lines represent the theoretical data of Pal et al. [51], computed using a JK semiempirical approach.

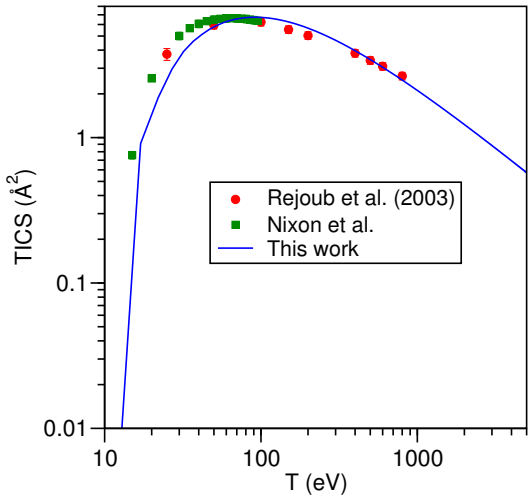

Figure 9. Electron-impact TICS for C_2H_5OH from threshold up to 5000 eV. The solid lines represent the TICS computed by numerically integrating the SDCS values. The filled circles and squares represent the experimental measurements of Nixon et al. and Rejoub et al., respectively [54,55].

3.9. DNA Constituents

Presented below are the scattering cross sections for pyrimidine (Py), tetrahydrofuran (THF), trimethylphosphate (TMP), and purine (PU). We compared the BEB-SDCS to the recommended data from the literature. Reliable cross sections for biomolecules such as these are important for track structure simulations such as PTra and the Geant4-DNA toolkit [56,57].

3.9.1. Pyrimidine ($C_4H_4N_2$)

Pyrimidine is the precursor to the three nucleic bases (cytosine, thymine, and uracil) of DNA and RNA. Thus, pyrimidine is a target of tremendous interest in the study of the interaction of radiation with biological matter [58]. The electron-impact ionization SDCS for pyrimidine are shown in Figure 10a–c. We compared our results with points that were derived by Bug et al. from experimental data with an error of the order 25% [59].

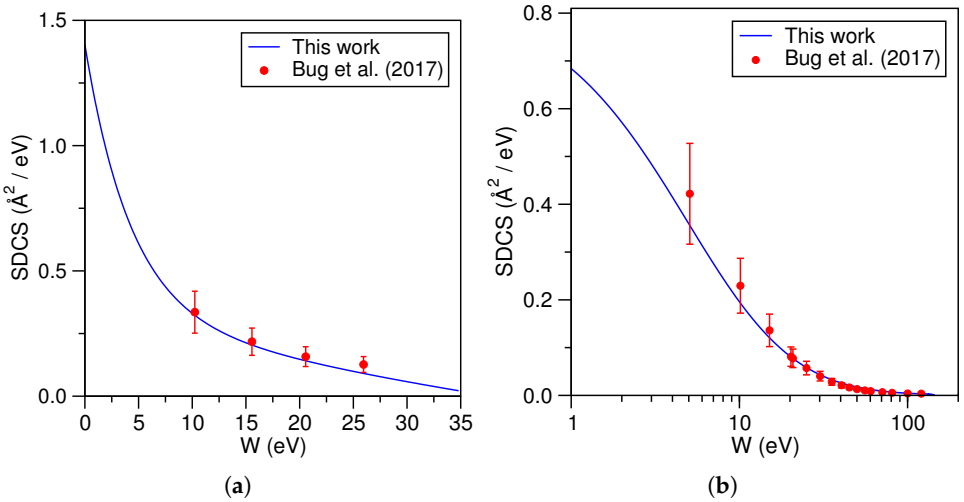

Figure 10. *Cont.*

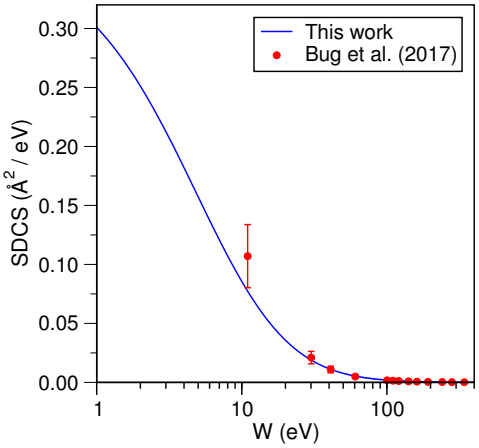

(**c**)

Figure 10. Electron-impact SDCS for pyrimidine at a primary electron energy of (**a**) T = 80 eV, (**b**) T = 300 eV, and (**c**) T = 1000 eV. The solid lines are the present results, and the filled circles are the experimental points derived by Bug et al. [59].

3.9.2. THF (C_4H_8O)

THF is a heterocyclic compound also known as oxolane. The THF molecule is a heterocyclic organic compound, which is a structural analogue of the deoxyribose group of DNA [59]. Thus, electron-impact cross sections for THF can be used to model the effect of ionizing radiation on genetic matter [60]. The results for THF are shown in Figure 11a–c. The values derived by Bug et al. from experimental data with an error in the order of 25% [59] are also shown.

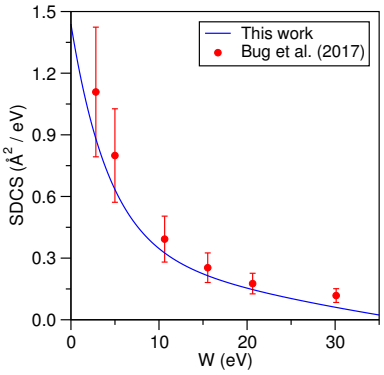

(**a**)

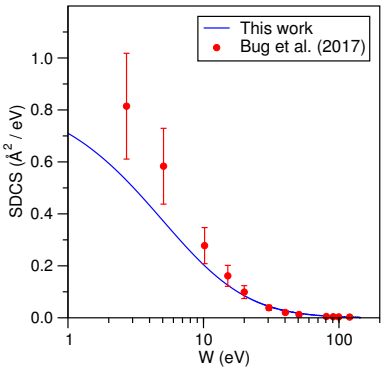

(**b**)

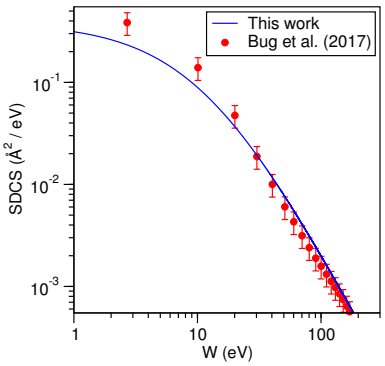

(**c**)

Figure 11. Electron-impact SDCS for THF at a primary electron energy of (**a**) T = 80 eV, (**b**) T = 300 eV, and (**c**) T = 1000 eV. The solid lines are the present results, and the filled circles are the experimental points derived by Bug et al. [59].

3.9.3. TMP ($C_3H_9O_4P$)

Trimethyl ester of phosphoric acid (TMP) is a structural analogue of the phosphate group of DNA, which is one-half of the sugar–phosphate backbone of the DNA double helix structure. The electron-impact ionization SDCS for TMP are shown in Figure 12a–c. Values derived by Bug et al. from the experimental data with an error in the order of 25% [59] are also shown.

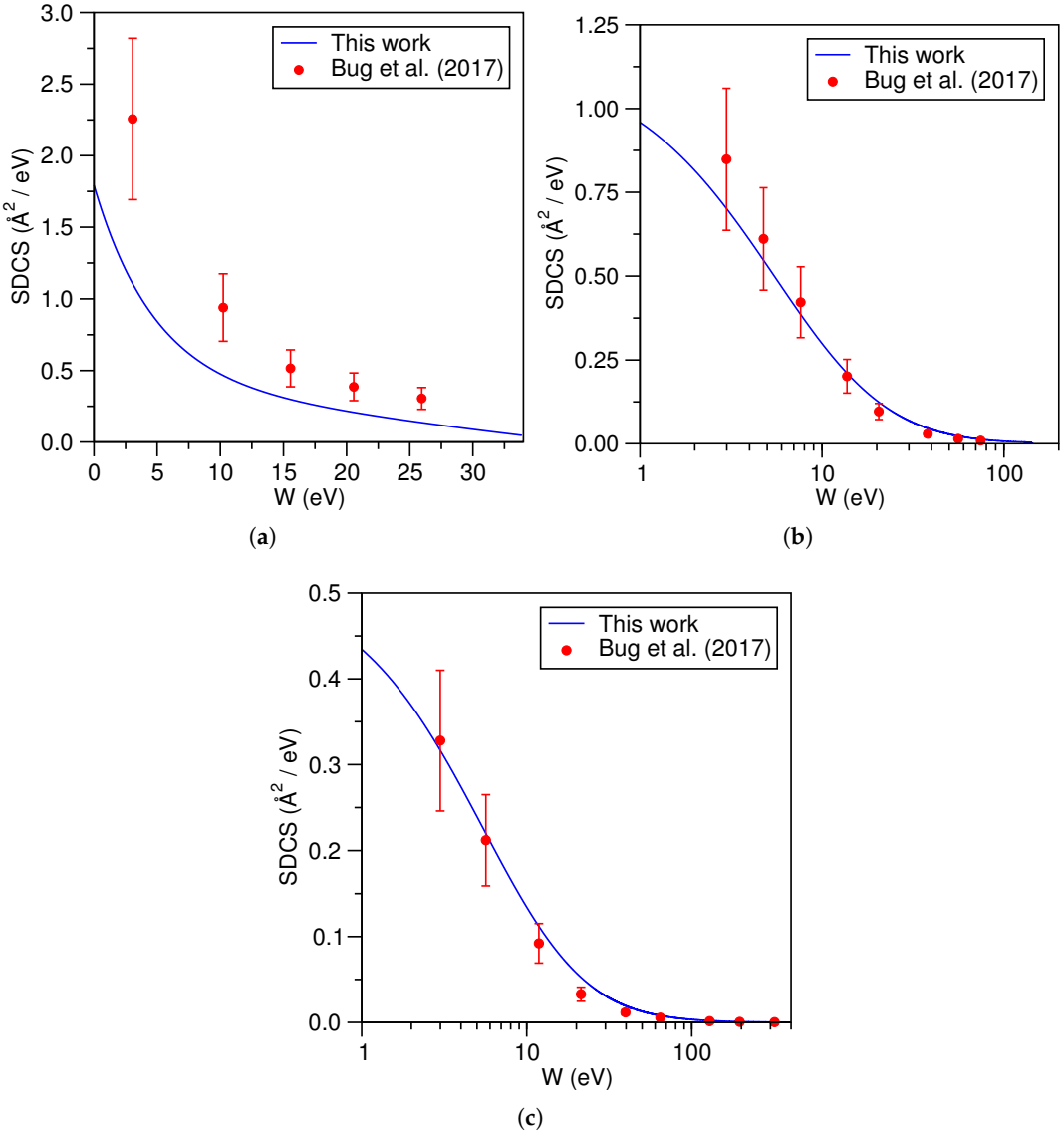

Figure 12. Electron-impact SDCS for TMP at a primary electron energy of (**a**) T = 80 eV, (**b**) T = 300 eV, and (**c**) T = 1000 eV. The solid lines are the present results, and the filled circles are the experimental points derived by Bug et al. [59].

3.9.4. Purine (C_5H_4N)

Purine is the structural precursor to adenine and guanine (two of the five canonical nucleobases). Thus, in the context of the ionization of DNA, purine is a very important target. Purine derivatives are also present in other biomolecules such as ATP and caffeine. The electron impact ionization SDCS for TMP are shown in Figure 13a. Since, experimental measurements of the SDCS were not available, we evaluated TICS in the primary energy range from threshold up to 5000 eV via numerical integration of the SDCS. The TICS then were compared to the recommended data of Bug et al. [59] as an indirect check on the SDCS. The TICS are shown in Figure 13b, and it can be seen that from 200 eV onwards the

agreement with the experiment was excellent. The maximum deviation in the magnitude of the BEB and experimental cross sections at the peak was about 20%, which is within the accepted range of uncertainty for BEB results.

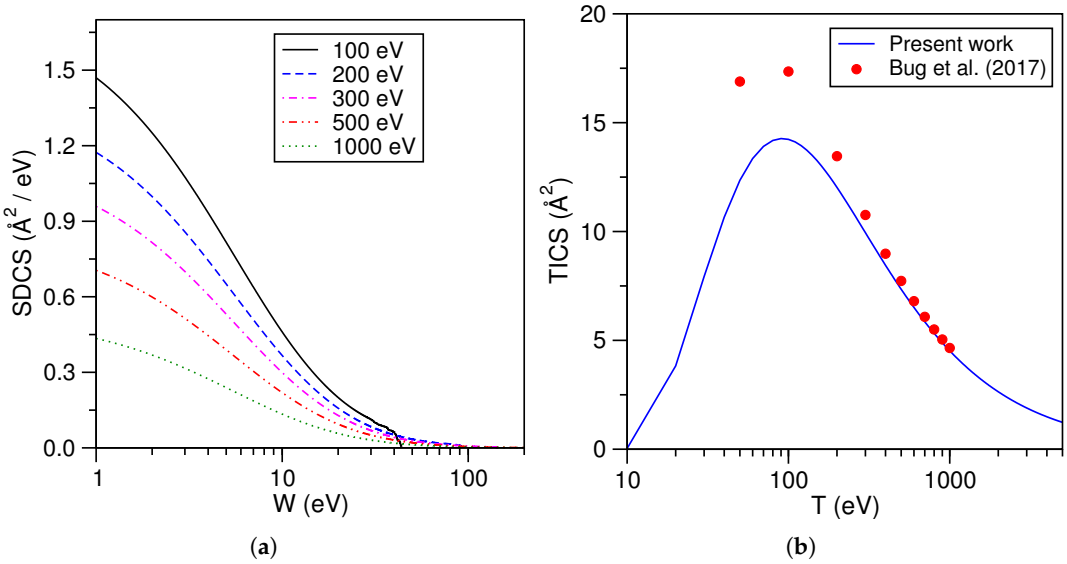

Figure 13. (**a**) Electron-impact SDCS for Purine at different primary electron energies. (**b**) TICS for electron-impact ionization of Purine in the primary electron energy range. The filled circles represent the recommended data points of Bug et al. [59].

3.10. Average Secondary Electron Energy

Average secondary electron energies, W_{av}, calculated via Equation (4) for the targets discussed throughout this work are shown in Figure 14a–d. It seems that there is some dependence of W_{av} on the geometrical size of the targets. Furthermore, it appears that at around 100 eV energy of the primary electron, the average energy of the secondary electron in almost all cases was around 10 eV with the exception of He. This artifact is due to the fact that the graphs are plotted on a large scale along the x-axis. In fact, the W_{av} as a function of incident energy, depends upon several factors such as the threshold energy, ionization cross sections, and SDCS. The inputs to calculate SDCS or TICS were B, U, N, and the experimental value of the ionization threshold. All the targets showed rising trends in W_{av} with an increase in incident energy from their respective thresholds. The SDCS were continuously decreasing with the increase in primary electron energy or secondary electron energy, whereas the TICS showed rising trends from the threshold until a maximum was reached; then, they start falling with further a increase in incident energy of the primary electron.

A better way to explain the variation in W_{av} with the number of electrons in the target is by invoking the Thomas-Reiche-Kuhn rule [61] for dipole transitions in a closed shell N-electron molecular system, according to which

$$\sum_i f_i + \int_0^\infty \frac{df}{dw} dw = N \tag{5}$$

where i ranges for ground to dipole-allowed excited states. It means that the ground and each excited state must be of opposite parity, which is due to the fact that a photon has one unit of angular momentum. The continuum oscillator strength integrated over W, is proportional to $N - \sum f_i$. This dependence is reflected in the variation of W_{av} with the number of electrons in the target in Figure 15.

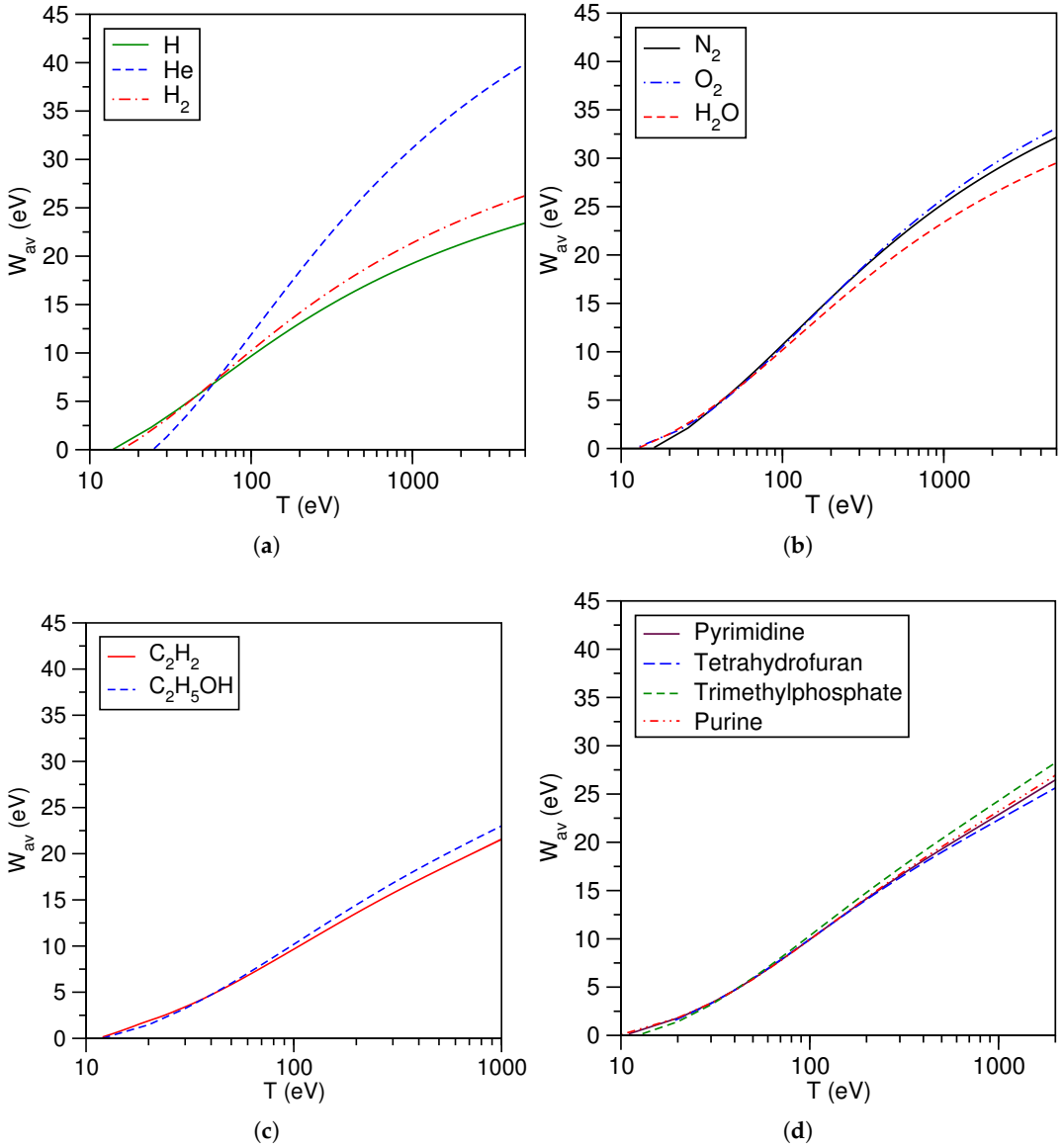

Figure 14. W_{av} for (**a**) hydrogen atom, helium, and hydrogen molecule, (**b**) nitrogen molecule, oxygen molecule, and water molecule, (**c**) acetylene and ethanol, and (**d**) pyrimidine, tetrahydrofuran, trimethylphosphate, and purine.

The SDCS computed for different targets showed a decreasing trend with an increase in secondary and primary electron energy. It means that the low energy electrons were produced due to electron impact even if the incident electron energy increased. The present SDCS results showed a good agreement with the ab initio convergent close-coupling data and experimental measurements. The deviations in the BEB and experimental results were observed near the threshold values. However, as the energy of the secondary electron increased, the present results showed a converging trend with the experimental data. The present BEB-based SDCS have limitations as well. They cannot reproduce the features such as resonances or estimate SDCS due to the dissociative ionization process [16]. However, the modified-BEB model [21,62,63] can be invoked to compute thge partial SDCS of cations and the energy deposited by them. These results were deliberately not shown, as there are no data to compare with the computed results. The present semiempirical approach not only yielded reliable results but was extremely simple to work with. It did not suffer from linear dependence or computational issues. The necessary input parameters were easily computed without posing a major challenge using any quantum chemistry

code. It would be interesting to apply the BEB model to compute the SDCS due to positron impact as the model has shown promising results for TICS [64–67].

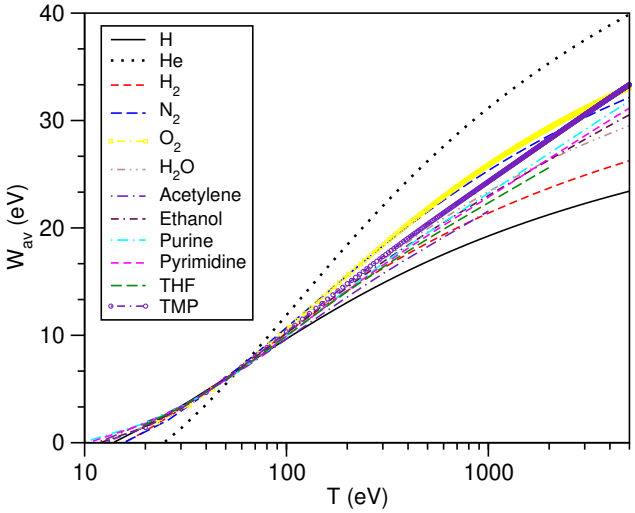

Figure 15. W_{av} for targets discussed throughout this work.

4. Discussion

The BEB model is fundamentally a high energy approximation. Thus, the results were expected to be in good agreement with the experimental measurements for high electron impact energies. This is in line with what we have shown in the present work. An encouraging aspect of the study has been that the BEB-SDCS compared very well with the latest CCC based results of Mori et al. [33]. The CCC theory relies on large basis sets, and the scattering wavefunction requires a large number of bound and continuum states. These features make the CCC approach extremely complicated and expensive to work with. For these reasons, its implementation on polyatomic targets has not been tested. The semiempirical approaches such as the BED and the JK both require the DOS as an input parameter. This hinders their general applicability.

In comparison, the BEB model has a simple analytical form, which works well with even modest computing resources. Thus, the present investigation establishes that the BEB model can be used for calculating the SDCS and various quantities of interest such as partial ionization cross sections (PICS) and W_{av}.

Author Contributions: Conceptualization, supervision, methodology, K.L.B., A.B., M.L., and K.G.; calculations, P.G.; writing the original draft, P.G.; review and editing, A.B., M.L., and K.G. All authors have read and agreed to the published version of the manuscript.

Funding: This research received no external funding

Institutional Review Board Statement: Not applicable.

Informed Consent Statement: Not applicable.

Data Availability Statement: The data can be obtained from the authors on request.

Acknowledgments: The authors are grateful to Nicolas A Mori and Satyendra Pal for providing numerical data of their work. P.G. is thankful to the Principal, BCAS for providing the necessary support to carry out the study. A.B, M.L., and P.G. also express their gratitude to the Department of Biotechnology (DBT) (Ministry of Science and Technology, Govt. of India) for motivating teachers and students to carry out scientific research at the undergraduate level under the star college status scheme.

Conflicts of Interest: The authors declare no conflict of interest.

Sample Availability: Not applicable.

Abbreviations

BED	binary-encounter-dipole
BEB	binary-encounter-Bethe
SE	Static-Exchange
CC	Close Coupling
CCC	Convergent Close Coupling
SDCS	Singly Differentiated Cross Sections
PICS	Partial Ionization Cross Sections
TICS	Total Ionization Cross Sections
DOS	Differential Oscillator Strength
JK	Jain-Khare
MO	Molecular Orbitals
eV	electron volt

References

1. Joshipura, K.N.; Mason, N. *Atomic-Molecular Ionization by Electron Scattering: Theory and Applications*; Cambridge University Press: Cambridge, UK, 2019. [CrossRef]
2. Märk, T.D.; Dunn, G.H. *Electron Impact Ionization*; Springer: Vienna, Austria, 1985. [CrossRef]
3. Caleman, C.; Ortiz, C.; Marklund, E.; Bultmark, F.; Gabrysch, M.; Parak, F.; Hajdu, J.; Klintenberg, M.; Timneanu, N. Radiation damage in biological material: Electronic properties and electron impact ionization in urea. *EPL* **2008**, *85*, 18005. [CrossRef]
4. Lillis, R.J.; Fang, X. Electron impact ionization in the Martian atmosphere: Interplay between scattering and crustal magnetic field effects. *J. Geophys. Res. Planets* **2015**, *120*, 1332–1345. [CrossRef]
5. Campbell, L.; Brunger, M. Electron collisions in atmospheres. *Int. Rev. Phys. Chem.* **2016**, *35*, 297–351. [CrossRef]
6. Adamovich, I.; Baalrud, S.D.; Bogaerts, A.; Bruggeman, P.J.; Cappelli, M.; Colombo, V.; Czarnetzki, U.; Ebert, U.; Eden, J.G.; Favia, P.; et al. The 2017 Plasma Roadmap: Low temperature plasma science and technology. *J. Phys. D Appl. Phys.* **2017**, *50*, 323001. [CrossRef]
7. Christophorou, L.G.; Olthoff, J.K. *Fundamental Electron Interactions with Plasma Processing Gases*; Springer: New York, NY, USA, 2012.
8. Kai, T. Single-differential and integral cross sections for electron-impact ionization for the damage of carbon clusters irradiated with X-ray free-electron lasers. *Phys. Rev. A* **2010**, *81*, 023201. [CrossRef]
9. Sanche, L. Low Energy Electron-Driven Damage in Biomolecules. *Eur. Phys. J. D* **2005**, *35*, 367–390. [CrossRef]
10. Boudaïffa, B.; Coultier, P.; Hunting, D.; Huels, M.A.; Sanche, L. Resonant Formation of DNA Strand Breaks by Low-Energy (3 to 20 eV) Electrons. *Science* **2000**, *287*, 1658–1660. [CrossRef]
11. Bray, I. Convergent close-coupling approach to light and heavy projectile scattering on atomic and molecular hydrogen. *J. Phys. B At. Mol. Opt. Phys.* **2017**, *50*, 202001. [CrossRef]
12. Scarlett, L.H.; Savage, J.S.; Fursa, D.V.; Bray, I.; Zammit, M.C.; Schneider, B.I. Convergent close-coupling calculations of electrons scattering on electronically excited molecular hydrogen. *Phys. Rev. A* **2021**, *103*, 032802. [CrossRef]
13. Tennyson, J. Electron–molecule collision calculations using the R-matrix method. *Phys. Rep.* **2010**, *491*, 29–76. [CrossRef]
14. Zammit, M.C.; Fursa, D.V.; Savage, J.S.; Bray, I. Electron– and positron–molecule scattering: Development of the molecular convergent close-coupling method. *J. Phys. B At. Mol. Opt. Phys.* **2017**, *50*, 123001. [CrossRef]
15. Graves, V.; Cooper, B.; Tennyson, J. The efficient calculation of electron impact ionization cross sections with effective core potentials. *J. Chem. Phys.* **2021**, *154*, 114104. [CrossRef]
16. Kim, Y.K.; Rudd, M.E. Binary-encounter-dipole model for electron-impact ionization. *Phys. Rev. A* **1994**, *50*, 3954–3967. [CrossRef] [PubMed]
17. Kumar, M.; Pal, S. (e,2e) ionization cross-sections for C_4H_4O, C_4H_8O and C_6H_8O. *Int. J. Mass Spectrom.* **2021**, *468*, 116665. [CrossRef]
18. Singh, R.; Kumar, M.; Pal, S. Electron impact ionization cross sections for methylamines. *J. Electron Spectrosc. Relat. Phenom.* **2018**, *226*, 22–25. [CrossRef]
19. Deutsch, H.; Becker, K.; Probst, M.; Märk, T.D. Chapter 3 The Semiempirical Deutsch–Märk Formalism: A Versatile Approach for the Calculation of Electron-Impact Ionization Cross Sections of Atoms, Molecules, Ions, and Clusters. In *Advances in Atomic, Molecular, and Optical Physics*; Academic Press: Cambridge, MA, USA, 2009; Volume 57, pp. 87–155. [CrossRef]
20. Deutsch, H.; Becker, K.; Matt, S.; Märk, T.D. Theoretical determination of absolute electron-impact ionization cross sections of molecules. *Int. J. Mass Spectrom.* **2000**, *197*, 37–69. [CrossRef]
21. Bharadvaja, A.; Bassi, M.; Arora, A.; Baluja, K.L. Electron interactions with Tetramethylsilane from ionization threshold upto 5000 eV. *Plasma Sources Sci. Technol.* **2021**, *30*, 095012. [CrossRef]
22. Hamilton, J.R.; Tennyson, J.; Huang, S.; Kushner, M.J. Calculated cross sections for electron collisions with NF_3, NF_2 and NF with applications to remote plasma sources. *Plasma Sources Sci. Technol.* **2017**, *26*, 065010. [CrossRef]

23. Irikura, K.K. Semi-empirical estimation of ion-specific cross sections in electron ionization of molecules. *J. Chem. Phys.* **2016**, *145*, 224102. [CrossRef]
24. Tanaka, H.; Brunger, M.J.; Campbell, L.; Kato, H.; Hoshino, M.; Rau, A.R.P. Scaled plane-wave Born cross sections for atoms and molecules. *Rev. Mod. Phys.* **2016**, *88*, 025004. [CrossRef]
25. Vriens, L. Binary-Encounter Electron-Atom Collision Theory. *Phys. Rev.* **1966**, *141*, 88–92. [CrossRef]
26. Stone, P.; Kim, Y.-K. An Overview of the BEB Method for Electron-Impact Ionization of Atoms and Molecules. *Surf. Interface Anal.* **2005**, *37*, 966–968. [CrossRef]
27. Denifl, S.; Märk, T.; Scheier, P. The Role of Secondary Electrons in Radiation Damage. *Radiat. Damage Biomol. Syst.* **2012**, 45–58. [CrossRef]
28. Frisch, M.J.; Trucks, G.W.; Schlegel, H.B.; Scuseria, G.E.; Robb, M.A.; Cheeseman, J.R.; Scalmani, G.; Barone, V.; Petersson, G.A.; Nakatsuji, H.; et al. *Gaussian~16 Revision C.01*; Gaussian Inc.: Wallingford, CT, USA, 2016.
29. Janev, R.K.; Samm, U.; Reiter, D. *Collision Processes in Low-Temperature Hydrogen Plasmas*; Technical report, TIB Hannover: Hannover, Germany, 2003.
30. Barklem, P.; Belyaev, A.; Guitou, M.; Feautrier, N.; Gadéa, F.; Spielfiedel, A. On inelastic hydrogen atom collisions in stellar atmospheres. *Astron. Astrophys.* **2011**, *530*, 9. [CrossRef]
31. Feldman, W.C.; Phillips, J.L.; Gosling, J.T.; Isenberg, P.A. Electron impact ionization rates for interstellar H and He atoms near interplanetary shocks: Ulysses observations. *AIP Conf. Proc.* **1996**, *382*, 622–625. [CrossRef]
32. Shyn, T.W.; Sharp, W.E.; Kim, Y.K. Doubly differential cross sections of secondary electrons ejected from gases by electron impact: 25–250 eV on H_2. *Phys. Rev. A* **1981**, *24*, 79–88. [CrossRef]
33. Mori, N.A.; Utamuratov, R.; Fursa, D.V.; Zammit, M.C.; Bray, I. Calculation of the single differential cross section for electron-impact ionization of atoms and molecules. *J. Phys. B At. Mol. Opt. Phys.* **2020**, *54*, 015205. [CrossRef]
34. Shyn, T.W. Doubly differential cross sections of secondary electrons ejected from atomic hydrogen by electron impact. *Phys. Rev. A* **1992**, *45*, 2951–2956. [CrossRef]
35. Opal, C.; Beaty, E.; Peterson, W. Tables of secondary-electron-production cross sections. *At. Data Nucl. Data Tables* **1972**, *4*, 209–253. [CrossRef]
36. Röder, J.; Ehrhardt, H.; Bray, I.; Fursa, D.V. Absolute double differential cross sections for electron-impact ionization of helium. *J. Phys. B At. Mol. Opt. Phys.* **1997**, *30*, 1309–1322. [CrossRef]
37. Hunten, D.M. The production of N_2^+ in the atmosphere. *Planet. Space Sci.* **1963**, *10*, 37–45. [CrossRef]
38. Broadfoot, A.; Hunten, D. N_2^+ emission in the twilight. *Planet. Space Sci.* **1966**, *14*, 1303–1319. [CrossRef]
39. Pal, S.; Kumar, J.; Bhatt, P. Electron impact ionization cross-sections for the N_2 and O_2 molecules. *J. Electron Spectrosc. Relat. Phenom.* **2003**, *129*, 35–41. [CrossRef]
40. Seki, K.; Elphic, R.C.; Hirahara, M.; Terasawa, T.; Mukai, T. On atmospheric loss of oxygen ions from earth through magnetospheric processes. *Science* **2001**, *291*, 1939–1941. [CrossRef] [PubMed]
41. Newson, K.A.; Price, S.D. The formation and dissociation of the ozone dication. *Int. J. Mass Spectrom. Ion Process.* **1996**, *153*, 151–159. [CrossRef]
42. Itikawa, Y.; Mason, N. Cross Sections for Electron Collisions with Water Molecules. *J. Phys. Chem. Ref. Data* **2005**, *34*, 1–22. [CrossRef]
43. Verkhovtsev, A.; Traore, A.; Muñoz, A.; Blanco, F.; García, G. Modeling secondary particle tracks generated by intermediate- and low-energy protons in water with the Low-Energy Particle Track Simulation code. *Radiat. Phys. Chem.* **2017**, *130*, 371–378. [CrossRef]
44. Wiklund, K.; Fernández-Varea, J.; Lind, B. A Monte Carlo program for the analysis of low-energy electron tracks in liquid water. *Phys. Med. Biol.* **2011**, *56*, 1985–2003. [CrossRef]
45. Bolorizadeh, M.A.; Rudd, M.E. Angular and energy dependence of cross sections for ejection of electrons from water vapor. I. 50–2000-eV electron impact. *Phys. Rev. A* **1986**, *33*, 882–887. [CrossRef]
46. Chen, Y.; Zhang, H.; Zhu, Y.; Yu, D.; Tang, Z.; He, Y.; Wu, C.; Wang, J. A new method of fullerene production: Pyrolysis of acetylene in high-frequency thermal plasma. *Mater. Sci. Eng. B* **2002**, *95*, 29–32. [CrossRef]
47. De Bleecker, K.; Bogaerts, A.; Goedheer, W. Detailed modeling of hydrocarbon nanoparticle nucleation in acetylene discharges. *Phys. Rev. E* **2006**, *73*, 026405. [CrossRef]
48. Kaiser, R.I. Experimental Investigation on the formation of Carbon-Bearing Molecules in the Interstellar Medium via Neutral-Neutral Reaction. *Chem. Rev.* **2002**, *102*, 1309–1358. [CrossRef]
49. Stein, T.; Bera, P.P.; Lee, T.J.; Head-Gordon, M. Molecular growth upon ionization of van der Waals clusters containing HCCH and HCN is a pathway to prebiotic molecules. *Phys. Chem. Chem. Phys.* **2020**, *22*, 20337–20348. [CrossRef]
50. Huber, S.E.; Seebacher, J.; Kendl, A.; Reiter, D. Assessment of Hydrocarbon Electron-Impact Ionization Cross Section Measurements for Magnetic Fusion. *Contrib. Plasma Phys.* **2011**, *51*, 931–943. [CrossRef]
51. Pal, S.; Singh, R.; Kumar, M.; Kumar, N. Ionization cross-sections for C_2H_2 and C_2H_5OH by electron- impact. *Radiat. Phys. Chem.* **2020**, *173*, 108877. [CrossRef]
52. Lopes, M.C.; Pires, W.; Nixon, K.L.; Amorim, R.; Silva, D.; Fernandes, A.; Ghosh, S.; Jones, D.; Campbell, L.; Neves, R.; et al. Electron impact ionization and fragmentation of biofuels. *Eur. Phys. J. D* **2020**, *74*, 88. [CrossRef]

53. Perrero, J.; Enrique-Romero, J.; Martínez-Bachs, B.; Ceccarelli, C.; Balucani, N.; Ugliengo, P.; Rimola, A. Non-energetic Formation of Ethanol via CCH Reaction with Interstellar H_2O Ices. A Computational Chemistry Study. *ACS Earth Space Chem.* **2022**, *6*, 496–511. [CrossRef]
54. Nixon, K.L.; Pires, W.A.D.; Neves, R.; Duque, H.; Jones, D.B.; Brunger, M.J.; Lopes, M. Electron Impact Ionisation and Fragmentation of Methanol and Ethanol. *Int. J. Mass Spectrom.* **2016**, *404*, 48–59. [CrossRef]
55. Rejoub, R.; Morton, C.D.; Lindsay, B.G.; Stebbings, R.F. Electron-impact ionization of the simple alcohols. *J. Chem. Phys.* **2003**, *118*, 1756–1760. [CrossRef]
56. Bug, M.U.; Gargioni, E.; Nettelbeck, H.; Baek, W.Y.; Hilgers, G.; Rosenfeld, A.B.; Rabus, H. Ionization cross section data of nitrogen, methane, and propane for light ions and electrons and their suitability for use in track structure simulations. *Phys. Rev. E* **2013**, *88*, 043308. [CrossRef]
57. Incerti, S.; Baldacchino, G.; Bernal, M.; Capra, R.; Champion, C.; Francis, Z.; Guèye, P.; Mantero, A.; Mascialino, B.; Moretto, P.; et al. The GEANT4-DNA Project. *Int. J. Model. Simul. Sci. Comput.* **2010**, *1*, 157–178. [CrossRef]
58. Champion, C.; Quinto, M.A.; Weck, P.F. Electron- and proton-induced ionization of pyrimidine. *Eur. Phys. J. D* **2015**, *69*, 127. [CrossRef]
59. Bug, M.U.; Woon, Y.B.; Rabus, H.; Villagrasa, C.; Meylan, S.; Rosenfeld, A.B. An electron-impact cross section data set (10 eV–1 keV) of DNA constituents based on consistent experimental data: A requisite for Monte Carlo simulations. *Radiat. Phys. Chem.* **2017**, *130*, 459–479. [CrossRef]
60. Fuss, M.C.; Sanz, A.G.; Blanco, F.; Limão-Vieira, P.; Brunger, M.J.; García, G. Differential and integral electron scattering cross sections from tetrahydrofuran (THF) over a wide energy range: 1–10,000 eV. *Eur. Phys. J. D* **2014**, *68*, 161. [CrossRef]
61. Bethe, H.A.; Salpeter, E.E. *Quantum Mechanics of One- and Two-Electron Atoms*; Springer: Berlin/Heidelberg, Germany, 1957. [CrossRef]
62. Goswami, K.; Arora, A.K.; Bharadvaja, A.; Baluja, K.L. Electron impact partial ionization cross sections of methyl alcohol up to 5 keV using the mass spectrometry data. *Eur. Phys. J. D* **2021**, *75*, 228. [CrossRef]
63. Arora, A.K.; Gupta, K.K.; Goswami, K.; Bharadvaja, A.; Baluja, K.L. A binary-encounter-Bethe approach to compute electron-impact partial ionization cross sections of plasma relevant molecules such as hexamethyldisiloxane and silane. *Plasma Sources Sci. Technol.* **2022**, *31*, 015008. [CrossRef]
64. Fedus, K.; Karwasz, G.P. Binary-encounter dipole model for positron-impact direct ionization. *Phys. Rev. A* **2019**, *100*, 062702. [CrossRef]
65. Sahgal, V.; Bharadvaja, A.; Baluja, K.L. Positron-induced scattering of acetone from 0.1 eV to 5 keV. *J. Phys. B At. Mol. Opt. Phys.* **2021**, *54*, 075202. [CrossRef]
66. Arora, A.K.; Sahgal, V.; Gupta, K.K.; Bharadvaja, A.; Baluja, K.L. Positron-induced scattering from pentane isomers beyond ionization threshold. *Eur. Phys. J. D* **2021**, *75*, 259. [CrossRef]
67. Arora, A.K.; Sahgal, V.; Bharadvaja, A.; Baluja, K.L. Positron-impact scattering off 1-1 $C_2H_2F_2$ from 0.1 eV to 4 keV. *Phys. Rev. A* **2021**, *104*, 022816. [CrossRef]